Available online at www.CivileJournal.org

Civil Engineering Journal

(E-ISSN: 2476-3055; ISSN: 2676-6957)

Vol. 12, No. 04, April, 2026

Performance Assessment of Secant Pile Walls in Deep Excavations Using 3D Numerical Modeling and Monitoring Data

Indra Noer Hamdhan [1, 2*], Masyhur Irsyam [3], Agus Himawan [4], Sinatra Prasetyo [5], Rinaldi Alamsyah [2]

[1] *Department of Civil Engineering, Institut Teknologi Nasional Bandung, Bandung 40124, Indonesia.*

[2] *National Geotechnics Center Itenas, Institut Teknologi Nasional Bandung, Bandung 40124, Indonesia.*

[3] *Department of Civil Engineering, Institut Teknologi Bandung, Bandung 40132, Indonesia.*

[4] *Geotechnical Consultant, Promisco Sinergi Indonesia, Bandung 40191, Indonesia.*

[5] *General Contractor, Wijaya Karya (Persero), Jakarta 13340, Indonesia.*

Received 25 June 2025; Revised 18 February 2026; Accepted 02 March 2026; Published 01 April 2026

Abstract

This study aims to evaluate the deformation behavior and internal forces of a secant pile retaining system used for deep excavation at the Sentiong Water Pump House project in North Jakarta. A three-dimensional numerical analysis was conducted using PLAXIS 3D to simulate excavation stages, groundwater conditions, and construction sequences, including secant pile installation, dewatering, strut and ground anchor installation, and structural loading. Soil parameters were derived from field and laboratory investigations and calibrated using inclinometer monitoring data. The analysis results indicate that the maximum horizontal deformation on the north side of the excavation reached 30.60 mm during the pre-stressing of the second ground anchor, which slightly exceeded the allowable limit specified in SNI 8460:2017. On the south side, the maximum horizontal deformation reached 126.3 mm during ground anchor installation, significantly exceeding the permissible deformation limit. These results demonstrate that while the secant pile system on the north side performed near the allowable threshold, the south-side retaining system exhibited insufficient stiffness and stability under combined excavation and groundwater effects. The novelty of this study lies in the integration of detailed construction-stage modeling, field monitoring calibration, and direct evaluation against national deformation criteria, providing practical insights for improving secant pile design and excavation safety in soft soil and high groundwater conditions.

Keywords: Secant Pile; Deformation; Internal Forces; Excavation; Plaxis 3D.

1. Introduction

In geotechnical construction, retaining walls play a critical role in maintaining soil stability, particularly in projects involving deep excavations or unfavorable ground conditions. Excavation activities inevitably alter the stress–strain state of the surrounding soil, potentially causing ground deformation and damage to nearby structures [1]. These excavation-induced effects are influenced by soil properties, excavation support systems, construction sequences, and excavation geometry [2–7]. Recent studies on deep excavations and secant pile-supported retaining systems have highlighted the importance of numerical modeling in capturing complex soil–structure interaction, especially under soft soil and high groundwater conditions. Secant pile walls are widely used due to their high stiffness and ability to resist lateral earth pressure while minimizing groundwater seepage, making them suitable for such challenging environments.

* Corresponding author: indranh@itenas.ac.id

https://doi.org/10.28991/CEJ-2026-012-04-015

Recent research has increasingly employed advanced three-dimensional (3D) numerical analyses and field monitoring to improve the prediction of excavation-induced deformation. Data-driven and field-calibrated 3D finite element frameworks have been developed to evaluate deformation responses in deep excavations near existing structures, integrating numerical modeling with monitoring data [8]. In addition, detailed instrumentation programs have been used to investigate the deformation behavior of secant pile walls in layered soil–rock profiles, emphasizing the influence of soil stiffness and three-dimensional effects [9]. Other emerging studies explore AI-assisted multi-model approaches to assess groundwater-responsive pile behavior, indicating a trend toward more holistic modeling strategies in geotechnical engineering practice [10]. Despite these advances, most existing studies still rely on two-dimensional analyses or uncalibrated numerical models and primarily focus on final excavation conditions. The availability of field-calibrated three-dimensional analyses and explicit evaluation of predicted deformation against national design standards remains limited. Direct comparison between calculated deformation and allowable limits specified in design codes is rarely addressed, reducing the practical applicability of many numerical studies for construction control and design verification.

In the Sentiong Water Pump House project in North Jakarta (Figure 1), secant piles were employed to stabilize excavations on both the north and south sides in close proximity to critical infrastructure such as elevated toll bridge piers. The project presents challenges related to variable subsurface conditions and excavation depths exceeding 8 m. To address the identified research gaps, this study evaluates the performance of the secant pile system using a field-calibrated three-dimensional numerical model developed in PLAXIS 3D. The analysis incorporates construction-stage effects and groundwater conditions, with model calibration based on field monitoring data. The results are directly assessed against the deformation limits specified in SNI 8460:2017 [11], providing a robust framework for evaluating excavation stability and construction safety.

Figure 1. Project of the Sentiong Pump House, North Jakarta

This paper is organized as follows. Section 2 describes the project background and geotechnical conditions. Section 3 presents the methodology, including soil parameter determination, numerical modeling, and calibration. Section 4 discusses the deformation and internal force results. Section 5 compares the findings with previous studies, and Section 6 presents the conclusions and recommendations.

2. Scope of Project

The modeling area in this analysis is limited to the area adjacent to one of the pillars of the elevated toll bridge, pillar P-216, using a modeling boundary limit of ½ the distance between pillars. A cross-section of the modeling plan can be seen in Figure 2. The location of the soil investigation that has been carried out is 7 points of SPT testing and 3 points of CPT testing as shown in Figure 3.

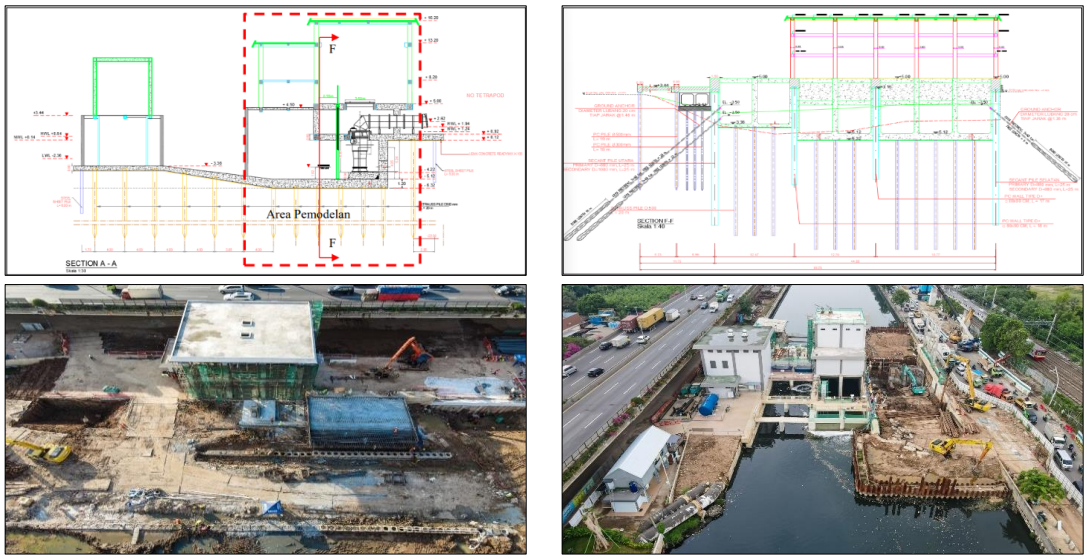

Figure 2. Cross section and long section modeling area

Figure 3. Layout project plan

3. Methodology

The methodology employed in this study is summarized in the workflow flowchart presented in Figure 4. The procedure includes site investigation and laboratory testing, soil parameter correlation, constitutive model selection, and the development of a three-dimensional numerical model using PLAXIS 3D. Excavation stages and construction sequences are simulated to realistically capture construction-stage effects, and the model is calibrated using inclinometer monitoring data. The calibrated model is subsequently used to evaluate ground deformation and internal forces in the secant pile system. In this study, SNI 8460:2017 is applied specifically as a deformation performance criterion within a serviceability-based evaluation framework. Accordingly, the numerical modeling adopts characteristic soil parameters without applying partial safety factors or ultimate load combinations, as the analysis is intended to assess deformation control and construction safety rather than ultimate limit state design.

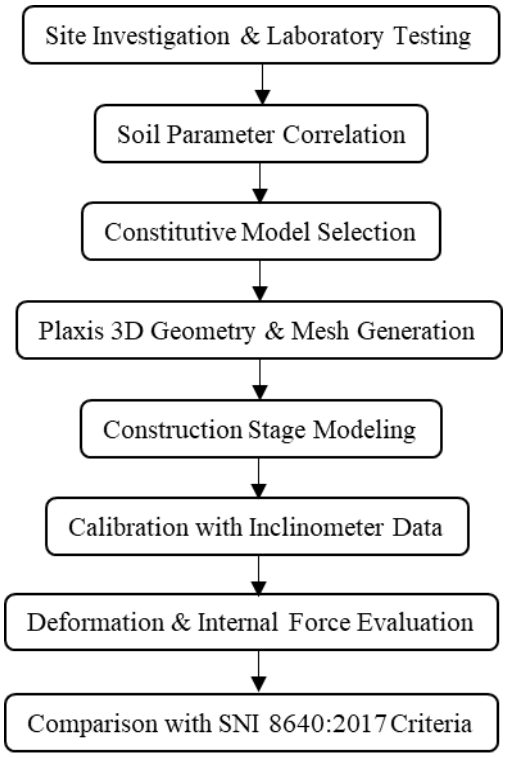

Figure 4. Methodological workflow of 3D numerical analysis and model calibration

3.1. Soil Parameters determination

Soil parameters were determined by integrating data from field investigations and laboratory testing to minimize uncertainty. Specifically, undrained shear strength was derived using the N-SPT correlation proposed by Terzaghi et al. [12] (see Figure 5), while the effective internal friction angle was determined based on the plasticity index relationship by Sørensen & Okkels (2013) [13] (see Figure 6). Furthermore, sensitivity checks were implicitly performed through calibration with inclinometer data, where stiffness parameters were adjusted to achieve agreement with measured deformations.

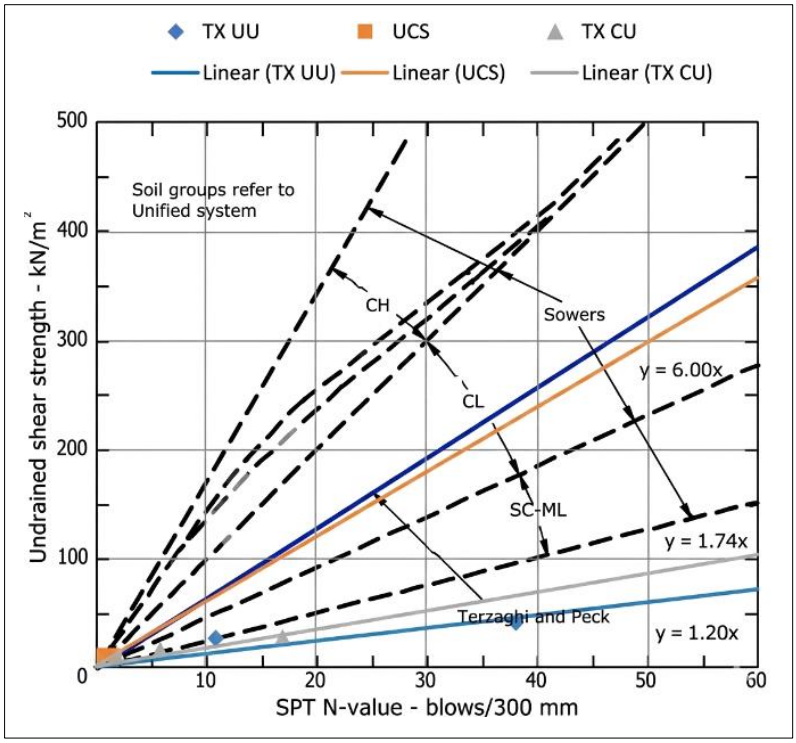

Figure 5. Plotting N-SPT vs undrained shear strength value from soil laboratory test

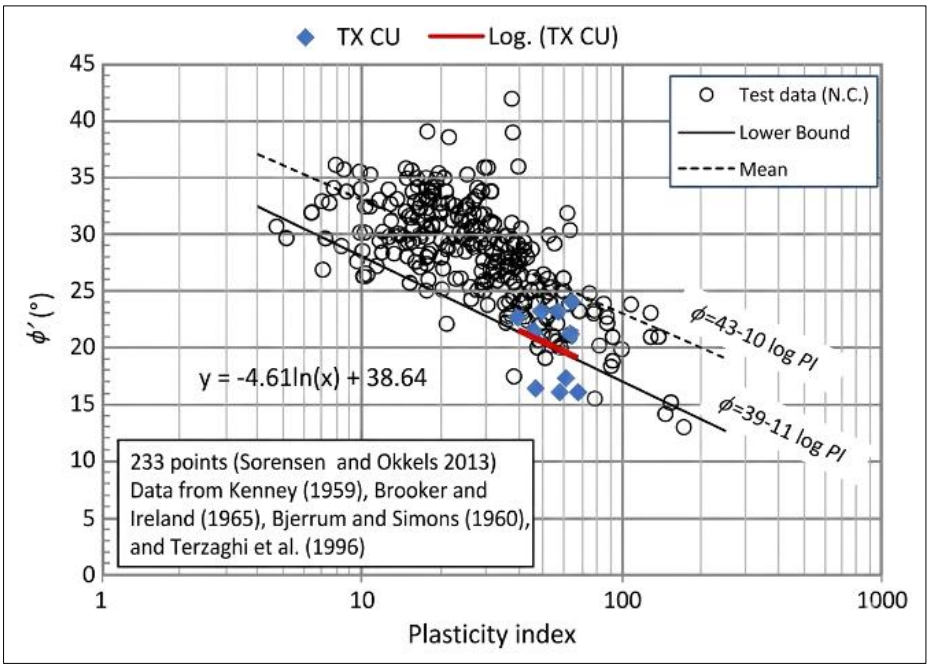

Figure 6. Plotting plasticity index vs effective friction angle value from soil laboratory test

3.2. Input Modeling Parameters

3.2.1. Soil Parameters

Soil parameters were derived from field and laboratory investigations, supplemented by correlations from existing references. For the numerical modeling, the Soft Soil (SS) model was adopted for layers with very soft to soft consistency, while the Hardening Soil (HS) model was utilized for stiffer soils (see Table 1). These constitutive models were selected over the Mohr–Coulomb model because they effectively capture stress-dependent stiffness, nonlinearity, and consolidation behavior—critical factors for deep excavations as highlighted by Law et al. (2014) [14]. The Mohr–Coulomb model was excluded to avoid the oversimplification inherent in its linear elastic–perfectly plastic formulation, which often underestimates excavation-induced displacements. The modeled soil stratigraphy (see Figure 7) was defined based on data from investigation points in close proximity to the project site.

Table 1. Soil parameters

Soil Parameters	1. Very Soft Clay	2. Soft Clay	3. Medium Stiff Silt	4. Hard Clayey Silt	5. Very Stiff Clayey Silt	Embankment	Unit
Soil model	SS model	SS model	SS model	HS model	HS model	HS model	-
Drainage type	Undrained A	Undrained A	Undrained A	Undrained A	Undrained A	Drained	-
Depth	0-8	8-12	12-16	16-29	29-35	-	m
Consistency	Very soft	Soft	Medium	Hard	Very Stiff	-	-
N-SPT design	1	2	6	44	28	-	-
γ_{unsat}	15.60	15.38	15.16	17.15	15.95	18.00	(kN/m^3)
γ_{sat}	16.60	16.38	16.16	16.15	16.95	18.00	(kN/m^3)
e_{init}	1.3	1	0.8	0.50	0.60	0.50	-
K_{ver}	0.00475	0.00475	0.00382	0.00423	0.00423	0.0864	m/day
K_{hor}	0.00475	0.00475	0.00382	0.00423	0.00423	0.0864	m/day
Cc	0.513	0.351	0.243	-	-	-	-
Cs	0.051	0.035	0.024	-	-	-	-
E_{50}^{ref}	-	-	-	87500	29400	30000	(kN/m^2)
E_{oed}^{ref}	-	-	-	70000	23520	24000	(kN/m^2)
E_{ur}^{ref}	-	-	-	262500	88200	90000	(kN/m^2)
c'	3.0	7.0	10.0	25.0	8.4	14.5	(kN/m^2)
phi'	23.0	23.0	25.0	32.0	26.0	30.0	°
ψ	0	0	0	2	0	0	°
R_{inter}	0.9	0.9	0.9	0.9	0.9	0.8	°

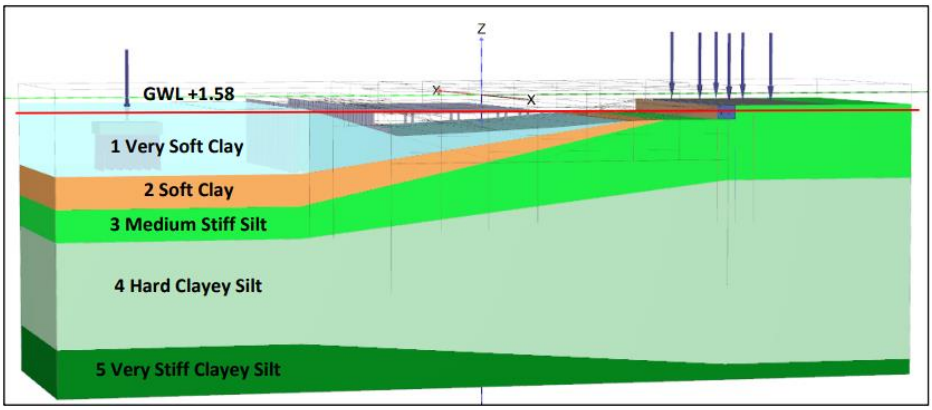

Figure 7. Geometry of soil stratigraphy

3.2.2. Structural Parameters of Deep Excavation Reinforcement

The reinforcement structures modeled for the excavation construction of the Sentiong pump house are foundation structures (PC Pile & Strauss Pile), wall structures (Secant pile & PC Wall) as shown in Figure 8, slab and pump house wall structures, ground anchor reinforcement, as well as temporary reinforcements such as SSP sheet piles and H beam type strut. Apart from that, there are also existing structures such as the flyover toll bridge foundation and CSSP sheet pile and ground anchor on the south side of the river. Detailed parameters only focus on secant pile parameters and additional ground anchor reinforcement (see Table 2 and 3).

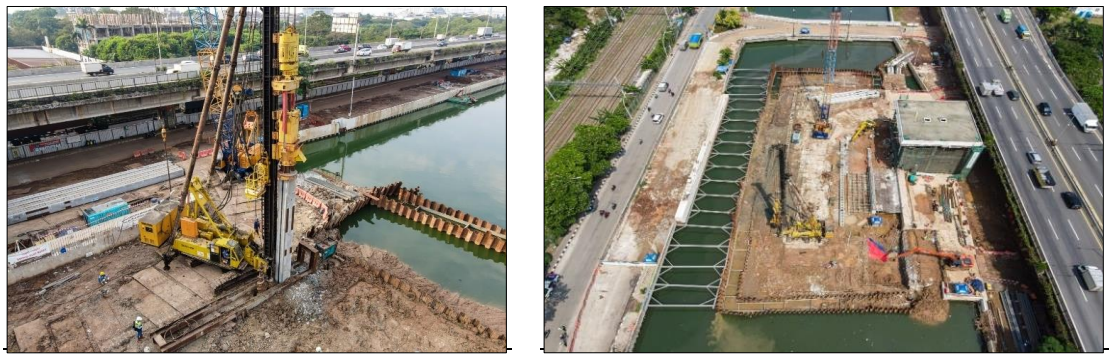

Figure 8. Installing PC Wall

Table 2. Detail parameters of secant pile

Parameter	Secant Pile Utara	Secant Pile Utara	Unit
Type	Plate	Plate	-
Concrete strength	Secondary fc' 30 Primary fc' 15	Secondary fc' 30 Primary fc' 15	MPa
d (thickness)	0.83	0.78	m
γ	24	24	(kN/m^3)
E	22.78×10^6	22.53×10^6	(kN/m^2)
ν	0.15	0.15	-

Table 3. Detail parameters of ground anchor

Parameter	Anchor Free Length	Anchor Bounded Length	Unit
Type	Node to Node Anchor	Embedded Beam	-
Beam Type	-	Massive Square	-
d (thickness)	-	0.2	m
γ	-	24	(kN/m^3)
E	200×10^6	30277632	(kN/m^2)
I_1	-	0.078543×10^{-3}	m^4
I_2	-	0.078543×10^{-3}	m^4
EA	196×10^3	-	(kN)
ν	-	0.15	-

In detailed modeling for secant piles as shown in Figure 9, equivalent of the input parameters as surface elements is required, with determination based on an equivalent approach which takes into account the cross-sectional area of the secant pile into a square cross-sectional area (see Figure 10) to obtain modeling input parameters as shown in Table 2.

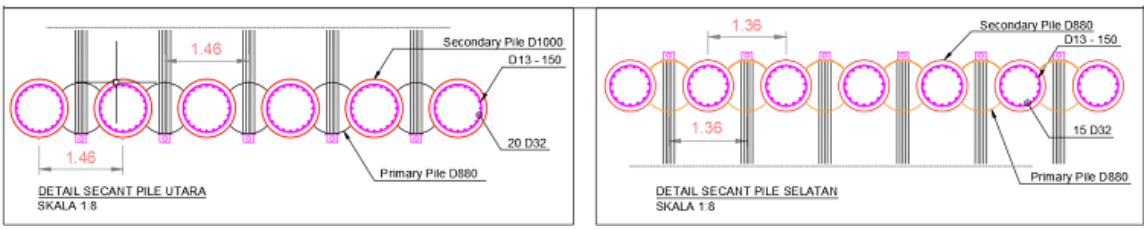

Figure 9. Detail drawing of secant pile

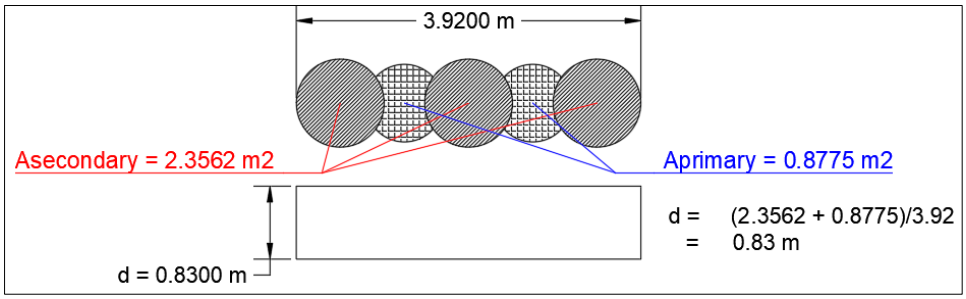

Figure 10. illustration of determining the equivalent parameters of a secant pile

The ground anchors are uses a low relaxation 7 strand anchor type with a planned grouting compressive strength of 40 MPa.

3.2.3. Load Input Parameters

The modeled load is the reaction load of placing the flyover toll bridge on the existing pile cap on the north side, the placement reaction can be seen in Table 4 and Figure 11. There is also a traffic load which refers to SNI 8460:2017 [11] for class I roads of 15 kPa as shown in Table 5.

Table 4. Load reaction to the pilecap of the existing toll bridge

Output Case	Case Type	F1 (cross-axis) (kN)	F2 (long-axis) (kN)	F3 (kN)	M1 (long-axis) (kN-m)	M2 (cross-axis) (kN-m)	M3 (kN-m)
SERV06	Combination	0	183	31901	2278	18323	0

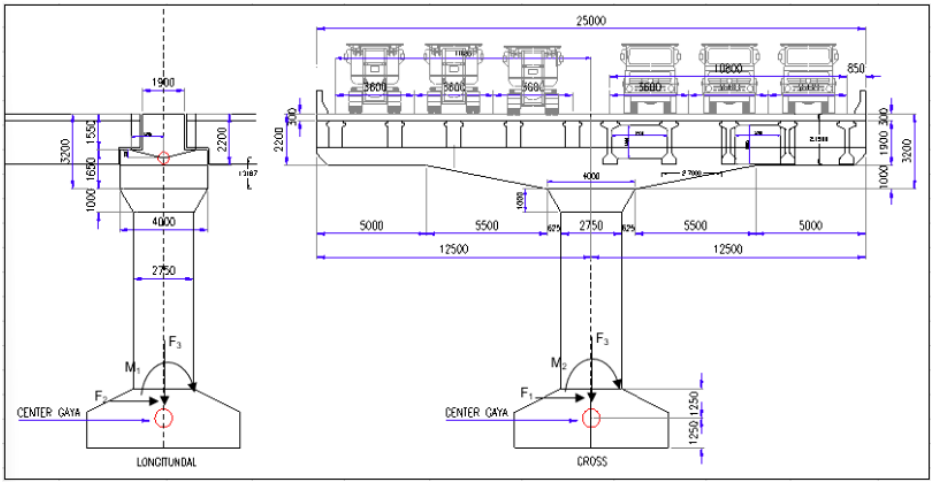

Figure 11. Schematic sign convention of load reaction

Table 5. Traffic load (source: SNI 8460:2017)

Road Class	Traffic Load (kPa)	Off-road Loads (kPa)
I	15	10
II	12	10
III	12	10

Other loads modeled include a construction load of 10 KPa and a BG28+Kelly heavy equipment load of 1250 kN with contact dimensions of 6 x 6 meters around the excavation site.

4. Calculation Method

To predict soil deformation that occurs around the excavation site during the construction process, numerical modeling analysis is needed. Modeling using a 2D analysis approach does not seem suitable, because due to the complex building structure conditions and also it cannot consider the effects of corners in the excavation area. As according to Ou et al. (1996) [15] and Finno et al. (2007) [16]. Therefore, this case analysis was carried out using a 3-dimensional approach, namely using PLAXIS 3D. The modeling carried out was only in the area adjacent to one of the existing pile caps of the flyover toll bridge, P-216, with boundary boundaries taken as ½ the distance between the other pile caps or a total boundary length of approximately ±35 meters.

4.1. Modeling of Geometry

The modeling geometry has existing conditions as shown in Figure 12. The element mesh uses a fine mesh, as explained by Derrick & Srivastava (2020) regarding the effect of mesh density on finite element analysis [17].

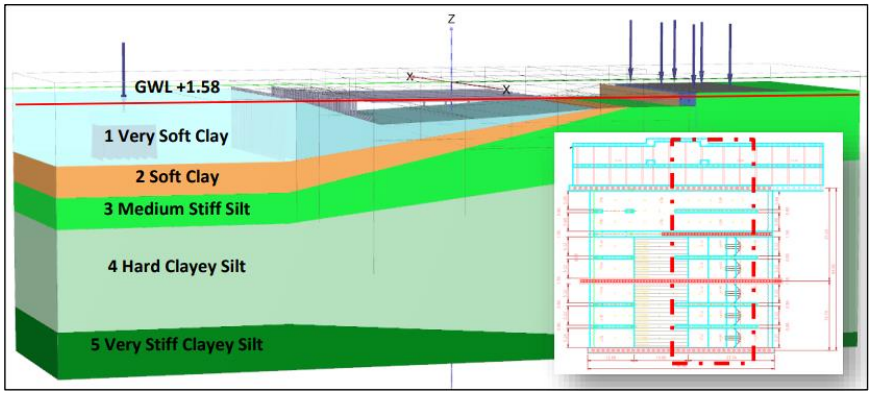

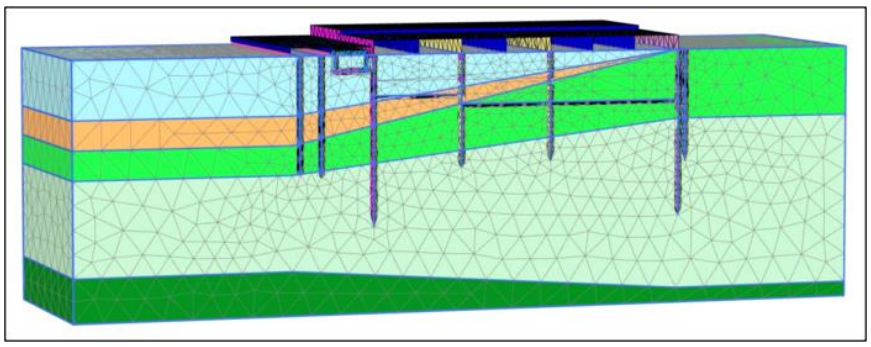

Figure 12. Geometry model and mesh element

4.2. Modeling Construction Stages

The modeling stage is using gravity loading for the initial condition stage and plastic analysis for all construction stages. Groundwater flow condition calculations use phreatic for stationary water level conditions and steady state for conditions where the excavation process is carried out assuming that dewatering has been carried out (see Table 6).

Table 6. PLAXIS modeling construction stages

No.	Description	Calculation type	Reset displacement to zero
1	Initial phase	Gravity loading	
2	Dredging excavation (El. -5.4 m)	Plastic	✓
3	Embankment fill at north side	Plastic	
4	Sheet pile (SSP) and PC pile installation at north side stage 1	Plastic	
5	Sheet pile (SSP) and PC pile installation at north side stage 2	Plastic	
6	Sheet pile (SSP) and PC pile installation at north side stage 3	Plastic	
7	Installation secant pile at north side stage 1	Plastic	
8	Installation secant pile at north side stage 2	Plastic	
9	Installation secant pile at north side stage 3	Plastic	
10	Excavation for installation box culvert at north side	Plastic	
11	Box culvert installation and re-fill embankment	Plastic	
12	Fill embankment at south side	Plastic	
13	Installation secant pile at south side stage 1	Plastic	
14	Installation secant pile at south side stage 2	Plastic	
15	Installation secant pile at south side stage 3	Plastic	
16	Installation PC wall for water pump house and uninstall sheet pile (SSP) north side	Plastic	
17	Dewatering and installation strut at north side stage 1	Plastic	
18	Installation ground anchor at north side stage 1	Plastic	
19	Pre-stress ground anchor north side stage 1	Plastic	
20	Excavation, dewatering and installation strut at north side stage 2	Plastic	
21	Installation ground anchor at north side stage 2	Plastic	
22	Pre-stress ground anchor north side stage 2	Plastic	
23	Installation base slab and strauss pile at north side stage 1	Plastic	
24	Excavation and dewatering at north side stage 3	Plastic	
25	Installation base slab and strauss pile at north side stage 2	Plastic	
26	Installation upper structure water pump house north side	Plastic	
27	Open the water flow on the north side	Plastic	
28	Excavation and dewatering at south side stage 1	Plastic	
29	Installation ground anchor at south side	Plastic	
30	Pre-stress ground anchor at south side	Plastic	
31	Excavation and dewatering at south side stage 2	Plastic	
32	Installation base slab and strauss pile at south side	Plastic	
33	Installation upper structure water pump house south side	Plastic	
34	Open the water flow on the south side	Plastic	

4.3. Calibration of PLAXIS 3D Modeling with Inclinometer Monitoring Results

Before evaluating the analysis results, model parameters were calibrated based on field monitoring to reduce uncertainty. The calibration focused on the installation of the SSP IV sheet pile and the northern PC pile (Stage 3), a phase identified as the most critical construction stage due to the maximum deformations observed. While the site progress encompasses embankment and spun pile works, selecting this controlling stage ensures the model captures the governing soil–structure interaction behavior necessary for a robust safety evaluation. The model was verified by simulating a cut at the inclinometer location, and the resulting calibration is shown in Figure 13.

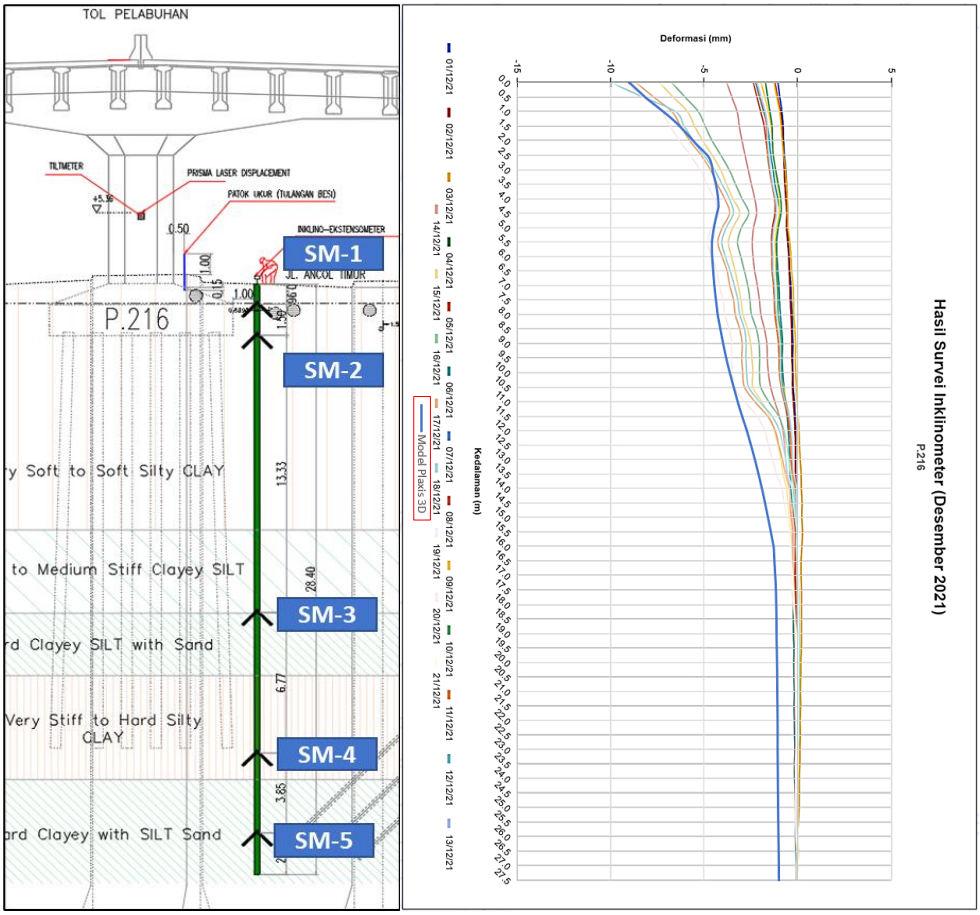

Figure 13. Result of modeling calibration with inclinometer monitoring data

4.4. Results of Three-Dimensional Numerical Modeling Analysis (PLAXIS 3D)

4.4.1. Results of Deformation and Internal force of Secant Pile on the North Side

Figure 14 illustrates the development of horizontal and vertical deformation along the secant pile wall under different construction and groundwater conditions. The results indicate contrasting deformation behaviors in the horizontal and vertical directions as construction progresses toward the operational stage. Horizontal deformation decreases with the activation of groundwater flow, while vertical deformation shows a gradual increase. This difference reflects the distinct mechanisms governing lateral wall movement and vertical soil–structure interaction during deep excavation.

4.4.1.1. Horizontal Deformation on the North Side Secant Pile

As shown in Figure 14, the maximum horizontal deformation of 30.60 mm occurs during the pre-stressed ground anchor installation on the north side, representing the most critical condition due to excavation-induced stress release and limited hydraulic counter-pressure. When groundwater flow is activated, the horizontal deformation reduces to 28.77 mm on the north side and further decreases to 15.84 mm in the final stage when groundwater flow on both sides is considered. This reduction indicates that groundwater pressure provides additional lateral confinement, reducing the net effective lateral earth pressure acting on the secant pile wall and improving overall excavation stability.

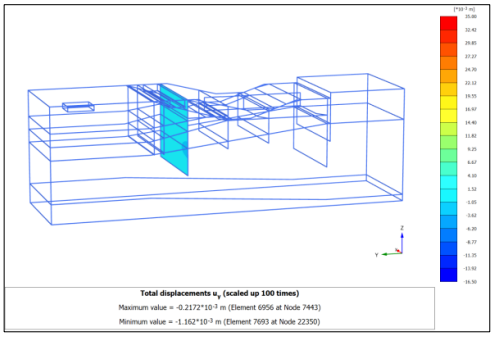

Phase of installation secant pile at south side stage 3

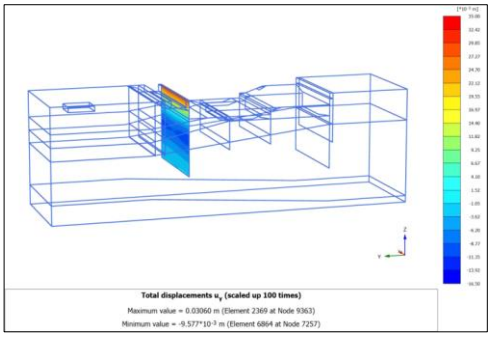

Phase of pre-stress ground anchor north side stage 2

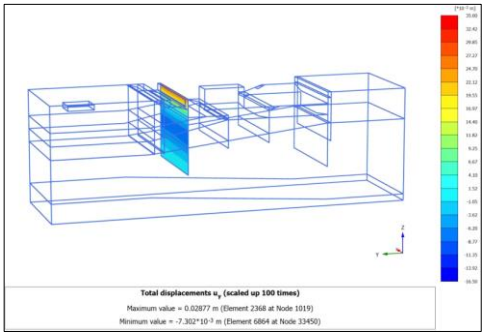

Phase of open the water flow on the north side

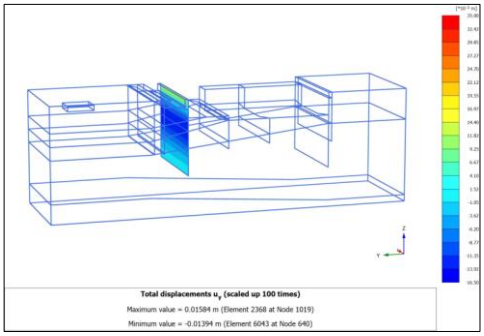

Phase of open the water flow on the south side

Figure 14. Horizontal deformations on the north side of the secant pile

4.4.1.2. Vertical Deformation on the North Side Secant Pile

In contrast, Figure 15 shows that vertical deformation increases with the activation of groundwater flow. During the pre-stressed ground anchor phase, the maximum vertical deformation reaches 14.28 mm, which increases to 18.38 mm when groundwater flow on the north side is activated and further rises to 19.11 mm when groundwater flow on both sides is considered. This behavior suggests that vertical deformation is influenced by changes in effective stress and seepage forces induced by groundwater flow, leading to additional vertical soil movement and consolidation effects. The combined results demonstrate that while groundwater activation plays a beneficial role in reducing horizontal deformation of the secant pile wall, it simultaneously contributes to increased vertical deformation, highlighting the importance of evaluating both deformation components to ensure a comprehensive assessment of excavation performance.

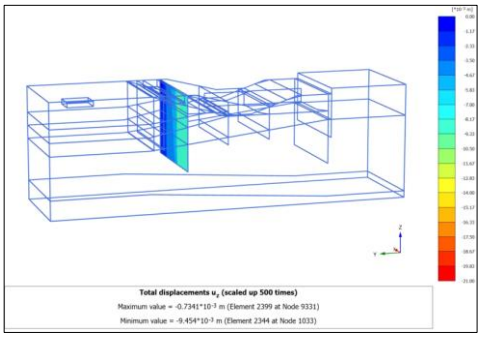

Stage of installation secant pile at south side stage 3

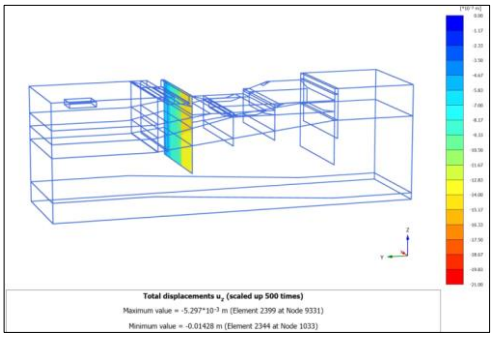

Stage of pre-stress ground anchor north side stage 2

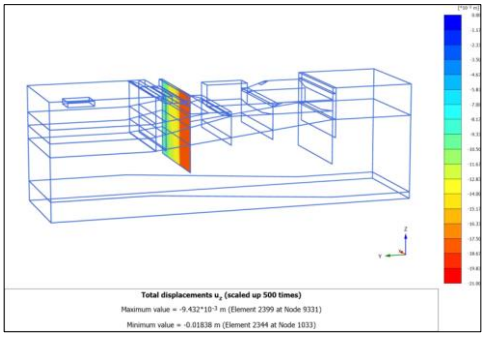

Phase of open the water flow on the north side

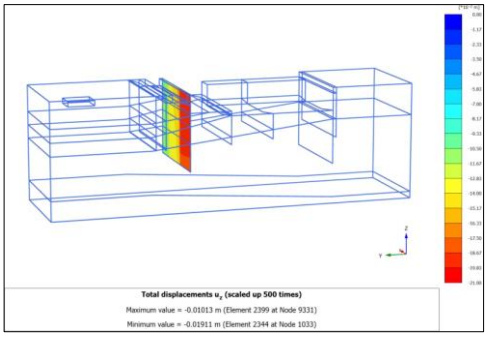

Phase of open the water flow on the south side

Figure 15. Vertical deformations on the north side of the secant pile

4.4.1.3. Internal Forces on the North Side Secant Pile

Figure 16 presents the internal force distribution along the secant pile wall in terms of axial force, shear force, and bending moment under different groundwater conditions. The results show that groundwater loading significantly affects the internal force response of the secant pile system. When groundwater flow is activated on the north side, the axial force ranges from 38.45 kN/m to –680.7 kN/m, while activation on both the north and south sides increases the axial force range to 59.47 kN/m and –652.7 kN/m. The shear force magnitude also increases with groundwater loading, from 320.5 kN/m and –165.3 kN/m to 376.3 kN/m and –216.7 kN/m, indicating greater lateral load transfer to the wall. Similarly, the bending moment increases due to the combined effects of soil pressure, structural reaction, and hydraulic loading, reaching 141.8 kN·m/m and –862.3 kN·m/m. These trends are consistent with previous studies, which reported that groundwater activation leads to increased axial force, shear force, and bending moment in retaining structures due to coupled soil–water interaction [18, 19]. Compared with earlier work, this study extends the existing knowledge by employing a field-calibrated three-dimensional numerical model with staged groundwater conditions, confirming the reliability and practical relevance of the obtained results.

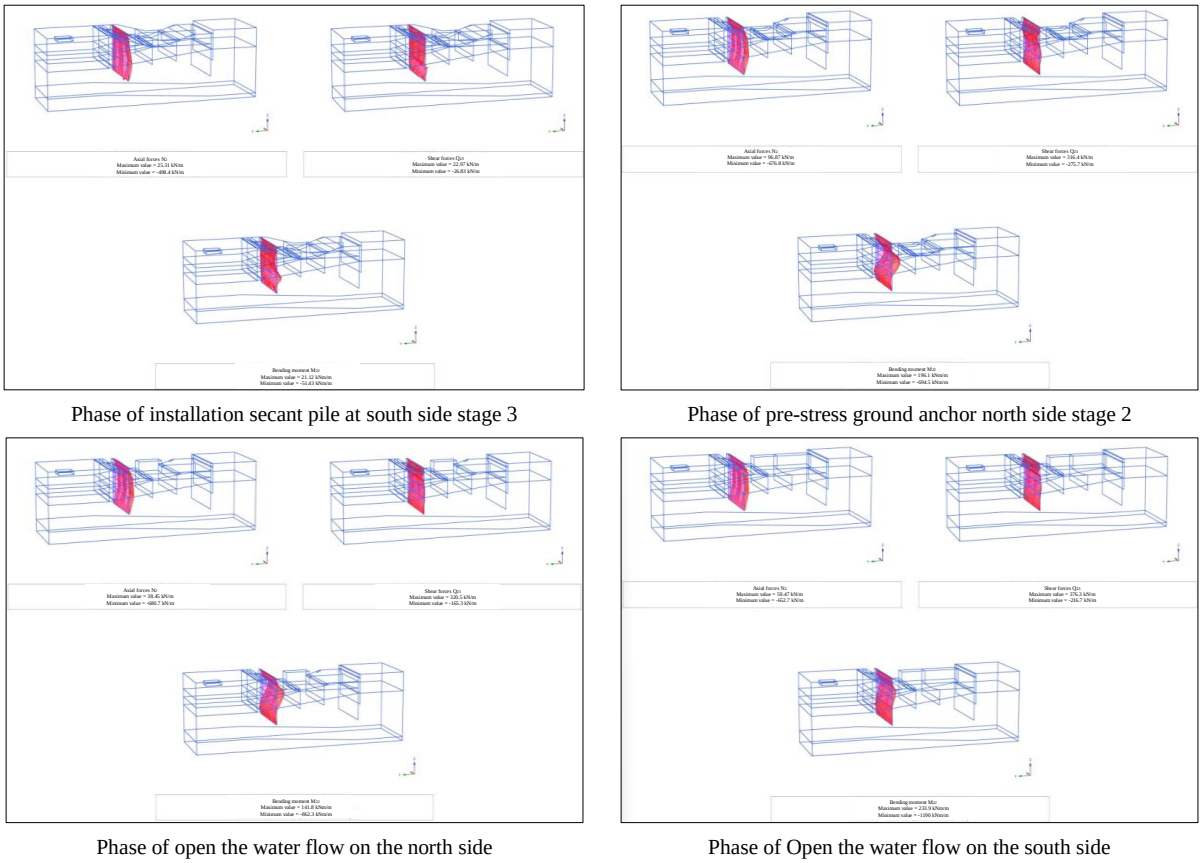

Phase of installation secant pile at south side stage 3

Phase of pre-stress ground anchor north side stage 2

Phase of open the water flow on the north side

Phase of Open the water flow on the south side

Figure 16. Internal forces on the north side of the secant pile

4.4.2. Results of Deformation and Internal Force of Secant Pile on the South Side

Deformation and internal forces are checked along the secant pile walls. The resulting deformation values are horizontal deformation, vertical deformation as well as forces in axial force, shear force and bending moment. These values are reviewed in the conditions where the northern secant pile was installed at the initial stage until the end of the pump house construction. The south side secant pile installation process is carried out after the north side secant pile is completed. Thus, the influence of deformation due to the previous stages is also taken into reviewing the south side secant pile analysis.

4.4.2.1. Horizontal Deformation on the South Side Secant Pile

Figure 17 shows the total horizontal deformation in the transverse river direction along the secant pile wall under different construction stages. When groundwater flow on the north side is activated, the maximum horizontal deformation is 23.53 mm. The deformation increases significantly to 126.3 mm during the pre-stressed ground anchor phase on the south side, representing the most critical condition prior to full anchorage effectiveness. In the final stage, with groundwater flow on both the north and south sides activated, the maximum horizontal deformation decreases to 111.0 mm. This reduction indicates that the ground anchors installed on the south side effectively restrain lateral deformation and mitigate the effects of groundwater loading on the secant pile wall.

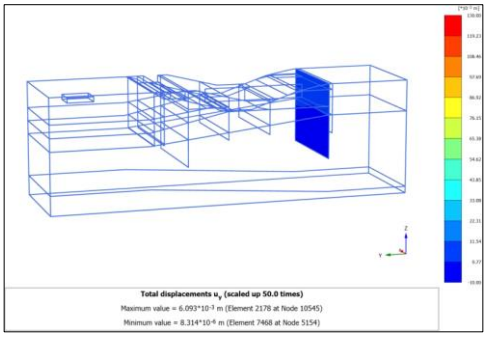

Phase of installation secant pile at south side stage 3

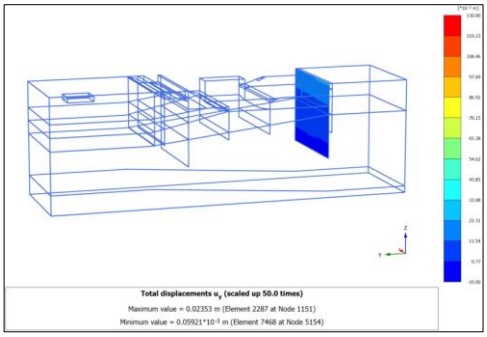

Phase of open the water flow on the north side

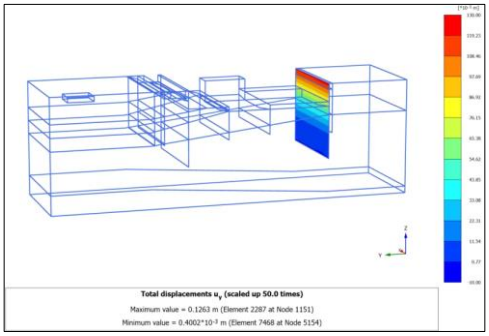

Phase of installation ground anchor at south side

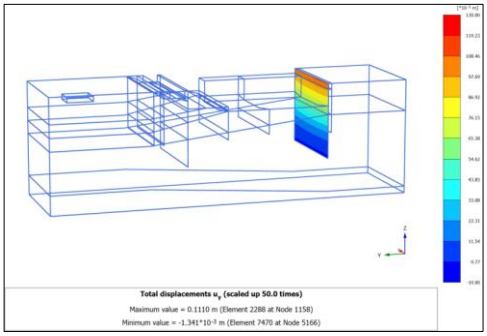

Phase of open the water flow on the south side

Figure 17. Horizontal deformations on the south side of the secant pile

4.4.2.2. Vertical Deformation on the South Side Secant Pile

Figure 18 shows the variation of total vertical deformation along the secant pile wall under different construction and groundwater conditions. Vertical deformation increases as construction progresses, from 5.60 mm when groundwater flow on the north side is activated to 6.75 mm during the pre-stressed ground anchor phase on the south side. A significant increase is observed in the final stage, where groundwater flow on both the north and south sides is activated, resulting in a maximum vertical deformation of 20.92 mm. This trend indicates that vertical deformation is strongly influenced by coupled soil–water interaction and seepage effects during the operational stage, highlighting the importance of incorporating realistic groundwater conditions in evaluating excavation performance.

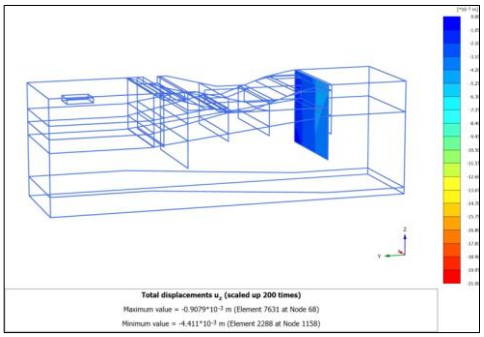

Phase of installation secant pile at south side stage 3

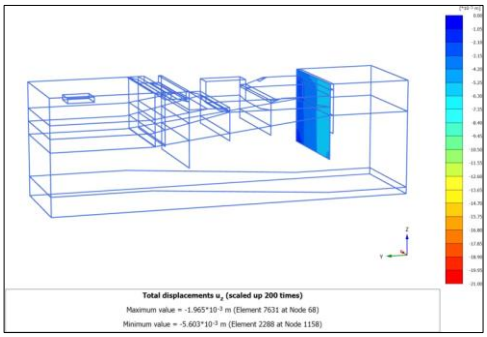

Phase of open the water flow on the north side

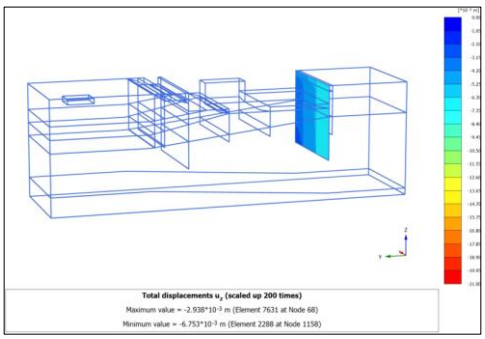

Phase of installation ground anchor at south side

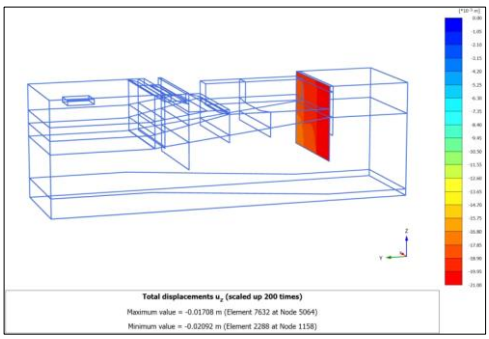

Phase of open the water flow on the south side

Figure 18. Vertical deformations on the south side of the secant pile

4.4.2.3. Internal Forces on The North Side Secant Pile

Figure 19 presents the internal forces distribution along the secant pile wall, including axial force, shear force, and bending moment, under combined groundwater loading from both the north and south sides. The results show that the axial force ranges from 197.6 kN/m to –1265 kN/m, indicating a significant contribution of hydraulic loading to compressive and tensile force development within the wall. Under the same condition, the shear force increases to 740.4 kN/m and –294 kN/m, reflecting enhanced lateral load transfer resulting from coupled soil and groundwater pressures. The bending moment also increases due to the combined effects of structural reaction, soil pressure, and groundwater loading, reaching a maximum of 702.5 kN·m/m and a minimum of –558.2 kN·m/m. These results demonstrate that groundwater flow from both sides represents the most critical loading condition for the secant pile wall and should be explicitly considered in internal force evaluation and design verification.

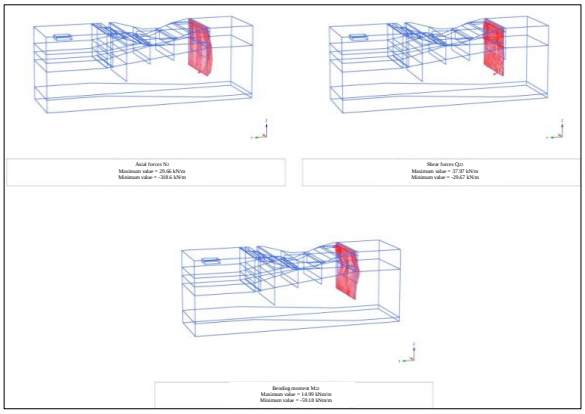

Phase of installation secant pile at south side stage 3

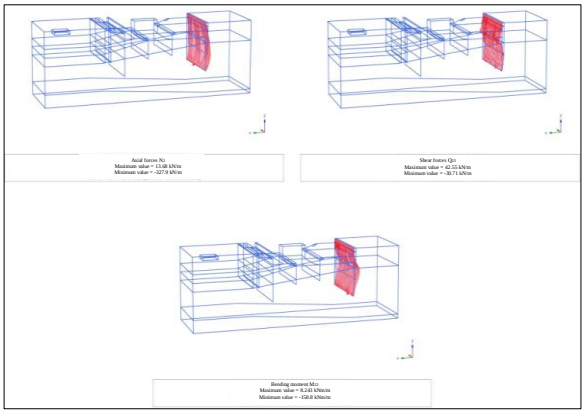

Phase of open the water flow on the north side

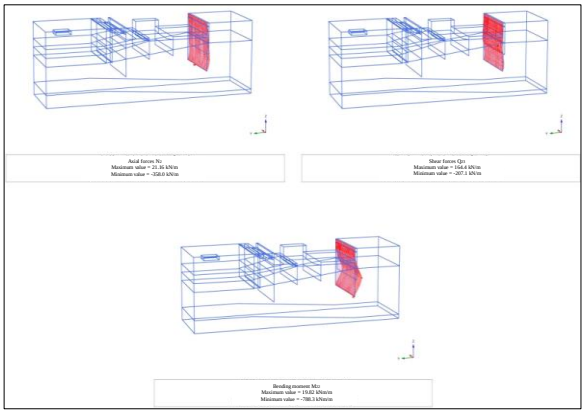

Phase of installation ground anchor at south side

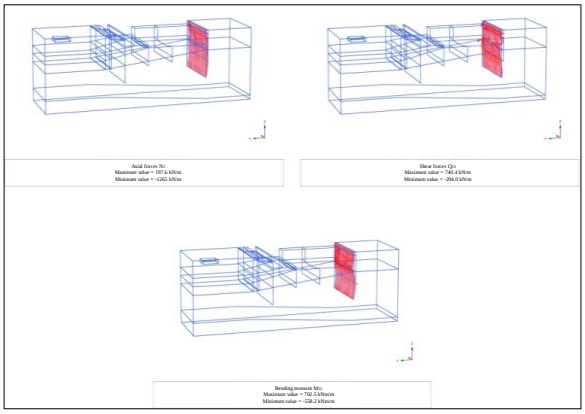

Phase of open the water flow on the south side

Figure 19. Internal forces on the south side of the secant pile

4.4.3. Summary of Results Analysis

Table 7 shows the recapitulation results of the deformation values and internal forces that occur along the secant pile wall. The horizontal deformation results summarized in Table 7 show that outward ground movement occurred prior to the installation of the secant pile wall due to excavation and embankment activities, particularly during the box culvert installation stage, with deformation values of approximately 7–9 mm. Following the installation of the secant pile wall (Stages 1–3), the deformation temporarily decreased or became negative, indicating that the retaining function of the secant pile had started to be effective. However, during subsequent excavation and dewatering stages, and before the complete installation of additional support systems such as ground anchors and struts, horizontal deformation increased significantly, especially on the south side, reaching a maximum of 126.3 mm. This behavior confirms that the performance of the secant pile wall is highly influenced by construction sequence, groundwater conditions, and the presence of complementary retaining systems. These observations are consistent with the overall conclusions of this study, which emphasize that the effectiveness of secant pile walls in deep excavation projects relies on integrated support systems, staged construction control, and realistic groundwater modeling to ensure deformation remains within acceptable limits.

Table 7. Recapitulation of total deformation in secant pile

No.	Description	North side		South side	
		Horizontal deformation (mm)	Vertical deformation (mm)	Horizontal deformation (mm)	Vertical deformation (mm)
1	Dredging excavation (El. -5.4 m)	-	-	-	-
2	Embankment fill at north side	-	-	-	-
3	Sheet pile (SSP) and PC pile installation at north side stage 1	-	-	-	-
4	Sheet pile (SSP) and PC pile installation at north side stage 2	-	-	-	-
5	Sheet pile (SSP) and PC pile installation at north side stage 3	-	-	-	-
6	Installation secant pile at north side stage 1	-0.58	-5.53	-	-
7	Installation secant pile at north side stage 2	-0.94	-8.4	-	-
8	Installation secant pile at north side stage 3	-1.16	-9.45	-	-
9	Excavation for installation box culvert at north side	7.17	-8.77	-	-
10	Box culvert installation and re-fill embankment	7.83	-9.67	-	-
11	Fill embankment at south side	9.06	-9.61	-	-
12	Installation secant pile at south side stage 1	9.28	-9.57	6.54	-2.37
13	Installation secant pile at south side stage 2	9.44	-9.53	8.65	-3.80
14	Installation secant pile at south side stage 3	9.56	-9.51	6.09	-4.41
15	Installation PC wall for water pump house and uninstall sheet pile (SSP) north side	3.89	-9.24	3.90	-4.14
16	Dewatering and installation strut at north side stage 1	-14.51	-8.85	17.60	-4.78
17	Installation ground anchor at north side stage 1	-14.51	-8.85	17.62	-4.78
18	Pre-stress ground anchor north side stage 1	17.00	-10.9	18.67	-4.88
19	Excavation, dewatering and installation strut at north side stage 2	17.18	-11.51	20.22	-6.01
20	Installation ground anchor at north side stage 2	17.18	-11.52	20.23	-6.02
21	Pre-stress ground anchor north side stage 2	30.60	-14.28	20.92	-6.10
22	Installation base slab and strauss pile at north side stage 1	29.91	-15.03	20.81	-6.02
23	Excavation and dewatering at north side stage 3	29.49	-15.75	23.27	-6.91
24	Installation base slab and strauss pile at north side stage 2	29.19	-15.36	23.23	-6.57
25	Installation upper structure water pump house north side	28.95	-16.8	23.03	-6.28
26	Open the water flow on the north side	28.77	-18.38	23.53	-5.60
27	Excavation and dewatering at south side stage 1	19.97	-19.46	126.30	-6.74
28	Installation ground anchor at south side	20.00	-19.46	126.30	-6.75
29	Pre-stress ground anchor at south side	19.97	-19.46	95.17	-9.08
30	Excavation and dewatering at south side stage 2	15.66	-20.3	109.90	-15.42
31	Installation base slab and strauss pile at south side	15.51	-19.87	111.10	-17.48
32	Installation upper structure water pump house south side	15.48	-19.61	111.10	-18.96
33	Open the water flow on the south side	15.84	-19.11	111.00	-20.92

Figure 20. Pump testing after construction

5. Conclusion

In this analysis, the deformation disparity results from a coupled effect rather than a single cause. While the geological transition from soft soil in the north to medium-stiff soil in the south is the primary driver of the settlement behavior, the construction history played a significant amplifying role. Specifically, the presence of a pre-existing platform embankment on the northern side altered the loading conditions, distinguishing it from the southern section where no such structure existed.

On the north side, the maximum horizontal deformation occurs during the pre-stress stage of the second ground anchor installation, reaching 30.60 mm. According to SNI 8460:2017 [11], the allowable horizontal deformation is limited to 0.5% of the excavation depth (H). With an excavation depth of approximately 6.0 m at this stage, the permissible deformation is 30 mm. The predicted deformation slightly exceeds this limit, indicating a marginal non-compliance with the standard and highlighting a critical construction stage that requires close monitoring and control.

On the south side, the deformation response is more critical. The maximum horizontal deformation of 126.3 mm occurs during the anchor installation stage, following excavation and dewatering to a depth of approximately 5.5 m. Based on SNI 8460:2017, the corresponding allowable deformation is 27.5 mm, which is substantially lower than the predicted value. This significant exceedance indicates that the secant pile wall alone is insufficient to control deformation under the combined effects of excavation and groundwater loading. The results confirm that the effectiveness of secant pile systems is highly dependent on construction sequencing, timely installation of ground anchors, and adequate groundwater control. Overall, this study demonstrates the importance of integrated support systems and field-calibrated three-dimensional numerical analysis to ensure deformation remains within acceptable limits and to maintain excavation safety and performance.

6. Declarations

6.1. Author Contributions

Conceptualization, I.H. and R.A.; methodology, I.H.; software, R.A.; validation, M.I., A.H. and S.P.; formal analysis, I.H. and R.A.; investigation, A.H.; resources, S.P.; writing—original draft preparation, I.H. and R.A.; writing—review and editing, I.H. and R.A; visualization, R.A.; supervision, S.P. All authors have read and agreed to the published version of the manuscript.

6.2. Data Availability Statement

The data presented in this study are available in the article.

6.3. Funding

The authors would like to express their sincere appreciation to the National Geotechnics Center Itenas, Institut Teknologi Nasional Bandung, for their financial support and for granting access to PLAXIS 3D software. This support was instrumental in facilitating the numerical modeling and contributing significantly to the outcomes of this research.

6.4. Conflicts of Interest

The authors declare no conflict of interest.

7. References

[1] Basmaji, B., Deck, O., & Al Heib, M. (2019). Analytical model to predict building deflections induced by ground movements. European Journal of Environmental and Civil Engineering, 23(3), 409–431. doi:10.1080/19648189.2017.1282382.

[2] Bryson, L. S., & Zapata-Medina, D. G. (2012). Method for Estimating System Stiffness for Excavation Support Walls. Journal of Geotechnical and Geoenvironmental Engineering, 138(9), 1104–1115. doi:10.1061/(asce)gt.1943-5606.0000683.

[3] Castaldo, P., Calvello, M., & Palazzo, B. (2013). Probabilistic analysis of excavation-induced damages to existing structures. Computers and Geotechnics, 53, 17–30. doi:10.1016/j.compgeo.2013.04.008.

[4] Cording, E. J., Long, J. L., Son, M., Laefer, D., & Ghahreman, B. (2010). Assessment of Excavation-Induced Building Damage. Earth Retention Conference, 3, 101–120. doi:10.1061/41128(384)7.

[5] Laefer, D. F., Ceribasi, S., Long, J. H., & Cording, E. J. (2009). Predicting RC Frame Response to Excavation-Induced Settlement. Journal of Geotechnical and Geoenvironmental Engineering, 135(11), 1605–1619. doi:10.1061/(asce)gt.1943-5606.0000128.

[6] Kim, S., & Finno, R. J. (2019). Inverse Analysis of a Supported Excavation in Chicago. Journal of Geotechnical and Geoenvironmental Engineering, 145(9), 04019050. doi:10.1061/(asce)gt.1943-5606.0002120.

[7] Zhang, W., Hou, Z., Goh, A. T. C., & Zhang, R. (2019). Estimation of strut forces for braced excavation in granular soils from numerical analysis and case histories. Computers and Geotechnics, 106, 286–295. doi:10.1016/j.compgeo.2018.11.006.

[8] Lai, F., Liu, S., Shiau, J., Liu, M., Cai, G., & Huang, M. (2025). Data-driven modeling for evaluating deformation of a deep excavation near existing tunnels. Underground Space, 24, 162–179. doi:10.1016/j.undsp.2025.04.003.

[9] Panagiotis, E., Rocchi, I., Petrella, F., Paulatto, E., & Zania, V. (2025). Deformation Behaviour of Secant Pile Walls in Layered Soil–Rock Profiles: Lessons Learned from Deep Excavations in Copenhagen. Geotechnical and Geological Engineering, 43(2), 119. doi:10.1007/s10706-025-03076-4.

[10] Bobade, M. V., & Malakar, P. (2026). AI-based real-time multi-model framework for groundwater-responsive pile behaviour. Journal of Engineering and Applied Science, 73(1). doi:10.1186/s44147-026-00874-2

[11] SNI 846:2017. (2017). Geotechnical Design Requirements. Standard Nasional Indonesia, Jakarta, Indonesia. (In Indonesian).

[12] Terzaghi, K., Peck, R. B., & Mesri, G. (1996). Soil mechanics in engineering practice. John Wiley & Sons, Hoboken, United States.

[13] Sørensen, K. K., & Okkels, N. (2013). Correlation between drained shear strength and plasticity index of undisturbed overconsolidated clays. Proceedings of the 18th international conference on soil mechanics and geotechnical engineering, 2-6 September 2013, Paris, France.

[14] Law, K., Roslan, H., & Zubaidah, I. (2014). 3D numerical analysis and performance of deep excavations in Kenny Hill formation. Numerical Methods in Geotechnical Engineering, 759–764. doi:10.1201/b17017-136.

[15] Ou, C.-Y., Chiou, D.-C., & Wu, T.-S. (1996). Three-Dimensional Finite Element Analysis of Deep Excavations. Journal of Geotechnical Engineering, 122(5), 337–345. doi:10.1061/(asce)0733-9410(1996)122:5(337).

[16] Finno, R. J., Blackburn, J. T., & Roboski, J. F. (2007). Three-Dimensional Effects for Supported Excavations in Clay. Journal of Geotechnical and Geoenvironmental Engineering, 133(1), 30–36. doi:10.1061/(asce)1090-0241(2007)133:1(30).

[17] Derrick, N., & Srivastava, A. K. (2020). Effect of mesh size on soil-structure interaction in finite element analysis. International Journal of Engineering Research & Technology, 96, 802-7. doi:10.17577/ijertv9is060655.

[18] Wang, C., Wang, B., Zhou, S., Wang, J., Li, X., & Xu, J. (2025). Influence of secant pile construction on the deformation of pile foundations in adjacent high-speed railway bridges. Geomechanics and Engineering, 40(5), 369-377.

[19] Richards, D. J., Wiggan, C. A., & Powrie, W. (2016). Seepage and pore pressures around contiguous pile retaining walls. Géotechnique, 66(7), 523–532. doi:10.1680/jgeot.14.p.121.